BIOCHEMISTRY
including biophysical chemistry & molecular biology

Article

pubs.acs.org/biochemistry

Solution Structure of a Complex of the Histidine Autokinase CheA with Its Substrate CheY

Guoya Mo, Hongjun Zhou, Tetsuya Kawamura, and Frederick W. Dahlquist*

Department of Chemistry and Biochemistry, University of California, Santa Barbara, California 93106-9510, United States

ABSTRACT: In the bacterial chemotaxis two-component signaling system, the histidine-containing phosphotransfer domain (the "P1" domain) of CheA receives a phosphoryl group from the catalytic domain (P4) of CheA and transfers it to the cognate response regulator (RR) CheY, which is docked by the P2 domain of CheA. Phosphorylated CheY then diffuses into the cytoplasm and interacts with the FliM moiety of the flagellar motors, thereby modulating the direction of flagellar rotation. Structures of various histidine phosphotransfer domains (HPt) complexed with their cognate RR domains have been reported. Unlike the *Escherichia coli* chemotaxis system, however, these systems lack the additional domains dedicated to binding to the response regulators, and the interaction of an HPt domain with an RR domain in the presence of such a domain has not been examined on a structural basis. In this study, we used modern nuclear magnetic resonance techniques to construct a model for the interaction of the *E. coli* CheA P1 domain (HPt) and CheY (RR) in the presence of the CheY-binding domain, P2. Our results indicate that the presence of P2 may lead to a slightly different relative orientation of the HPt and RR domains versus those seen in such complex structures previously reported.

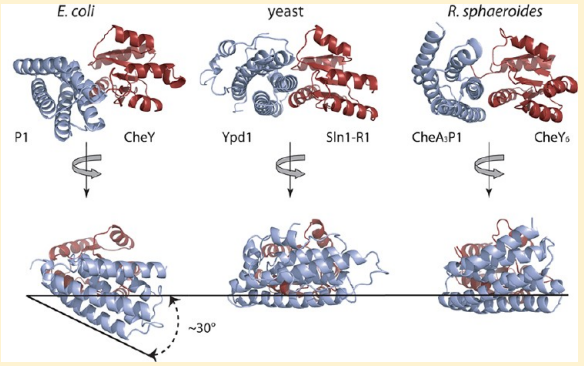

Motile bacteria propel themselves by the rotary motion of flagella, and they have the tendency to swim toward attractants and away from repellents, the behavior known as chemotaxis. The direction of the movement is determined by the sense of rotation of the flagellar motor, which is controlled by a complex two-component signal transduction system that senses the temporal concentration gradient of the attractants and repellents in their surroundings. The binding of such molecules by transmembrane chemoreceptors modulates the autophosphorylation activity of CheA (the histidine kinase, HK), the central kinase in the bacterial chemotactic signaling system. The increased level of autophosphorylation of CheA in the presence of negative stimuli results in an elevated level of phosphorylation of CheY, one of the two CheA substrates. Phosphorylation of CheY enhances its affinity for the FliM moiety of the flagellar motor. This interaction enhances the probability that the motor rotates clockwise, which leads to the tumbling motion of the cell and the resulting change in direction. In the presence of attractants, the CheA phosphorylation activity is inhibited, and the majority of CheY remains unphosphorylated, ensuring the counterclockwise rotation of the motor, which results in smooth swimming.[1−3]

CheA is a five-domain protein (Figure 1).[2,4] The functional unit of CheA is thought to be the dimeric form, and the dimerization is mediated by the P3 domain. The environmental signal input sensed by the chemoreceptor is transduced to CheA through its regulatory domain P5, which mediates the interaction of CheA with the receptor and the coupling protein, CheW. Signals from the receptor, upon the repellent ligand binding or attractant desorption, activates the kinase activity of CheA, and the histidine-containing phosphotransfer domain (HPt) P1 which receives a phosphoryl group from the ATP bound to the P4 domain. The P1 domain subsequently transfers the phosphoryl group to the cognate response regulator (RR) CheY. In *Escherichia coli* and related systems, CheY is bound to P2. A conformational change in CheY upon phosphorylation facilitates its dissociation from the P2 domain into the cytoplasm for the eventual interaction with the flagellar motors.[5,6]

While the structures and functions of the receptor, CheW, CheY, and the five CheA domains have been well established, the nature of the interactions through which the signal is relayed between these participants has been poorly understood. One of the unresolved issues is how the activated (phosphorylated) CheA P1 domain enhances the rate of CheY phosphorylation. It is known that CheY can be phosphorylated by small-molecule phosphodonors such as acetyl phosphate and phosphoimidazole, but the rates are slower by 3 orders of magnitude than the rate of phosphorylation by CheA.[7] The observed rate enhancement by CheA seems to be at least partially due to the enhanced local concentration of CheY around the phosphotransfer domain, P1. In CheA, P1 is connected to the CheY-binding domain (P2) by a 23-residue linker.[8] The P2 domain binds tightly to CheY, with a dissociation constant in the low micromolar range, and it can be estimated that the effective local

Received: February 1, 2012
Revised: April 6, 2012
Published: April 11, 2012

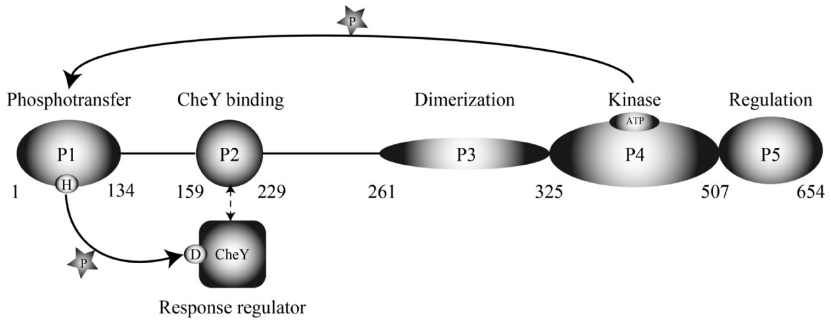

Figure 1. Histidine kinase CheA and CheY in *E. coli*. The function and residue numbers of each domain are shown. The solid arrows show the flow of phosphate transfer. The dashed arrow shows the interaction between the P2 domain and CheY.

concentration of CheY for the P1 domain is roughly 4 mM (see Discussion). However, the rate of phosphotransfer by CheA is still much faster than that by the small-molecule phosphodonors at a comparable concentration, and it seems obvious that the P1 domain plays an active role in the enhanced rate of phosphotransfer by CheA. The goal of this study is to provide a structural basis for the mechanism by which P1 accomplishes this.

Structures of various histidine phosphotransfer domains (HPt) complexed with their cognate RR have been reported.[9−12] Among them, *Rhodobacter sphaeroides* $CheA_3P1$ and $CheY_6$ are orthologs of *E. coli* P1 and CheY, and yeast Ypd1 and SLN1 (R1) are their structural homologues; possible clues for the mechanism of P1−CheY interaction have come from these crystal structures. In both cases, two major factors stabilizing the complex appear to be (1) the interaction between α-helix 1 of the RR domain and the helices equivalent to α-helix 1 of *E. coli* P1 and (2) the interaction of the helix containing the active site histidine of the HPt domain with the $\beta5-\alpha5$ loop of the RR. Do *E. coli* P1 and CheY employ a similar mode of interaction? One difference that sets the *E. coli* CheA−CheY system apart from these systems is the presence of the CheY-binding domain, P2, in *E. coli* CheA. This may affect the way P1 can orient itself against CheY in at least two ways. First, unlike the HPt domains in the systems used in the crystallographic studies mentioned above, where the HPt and RR domains provide all the affinity and specificity of the interaction, the *E. coli* system has an additional CheY-binding domain contributing specificity and affinity to the inherently low affinity of the P1−CheY interaction. Second, the linker connecting the two domains, while enhancing the effective concentration of CheY for P1, may also have a restricting effect on how P1 can sample the space around CheY.

To address these issues, we used the modern nuclear magnetic resonance (NMR) techniques to construct a structural model for the interaction between CheY and CheA P1P2 (where P1 is connected to P2 by the native linker). In this analysis, the P1 domain and CheY were docked as rigid bodies based on the short-range distance constraints provided by the nuclear Overhauser effect (NOE) measurements and long-range distance constraints provided by the paramagnetic relaxation enhancement measurements using the nitroxide spin-label MTSL.[13,14] We observed that the interaction between CheY and P1 is mediated through the interaction surfaces largely consistent with those observed in the crystal structures of the yeast Ypd1−SLN1(R1) complex and the *R. sphaeroides* $CheA_3P1-CheY_6$ complex. Our model indicates, however, in the presence of the linker and the P2 domain, the relative orientation of the HPt and RR may be slightly different from those seen in the previously reported HPt−RR crystal structures. We also show that the mutations affecting the P1−CheY interaction surface as observed by NMR had detrimental effects on the rate of phosphotransfer, as assessed by a single-turnover kinetic method, which suggests that the mode of interaction reported here is biochemically relevant.

MATERIALS AND METHODS

Protein Expression and Purification. Wild-type *E. coli* CheY (residues 1−129) was expressed in an *E. coli* K38 strain carrying the pCW expression plasmid.[15] The CheA P1 domain (residues 1−134) was cloned into pET28a (Novagen) at the *Nco*I and *Xho*I sites in frame with the C-terminal His_6 tag and expressed in BL21(DE3) (Novagen). The CheA P2 domain (residues 156−229) was also cloned into pET28a at the *Nco*I and *Xho*I sites in frame with the C-terminal His_6 tag and expressed in BL21(DE3). The CheA P1P2 fragment was expressed in BL21(DE3) carrying pREP4 and pRS1-4 (pQE12, CheA residues 1−223, C-terminal His_6 tag).[8,16] The CheA P3P4P5 fragment (residues 261−654) was cloned into pET28a with the N-terminal His_6 tag and expressed in BL21(DE3). All proteins were purified following the published protocols[8,15,17] or by Ni^{2+}-NTA chromatography (Qiagen).

P1 mutants F8A and E15A, P1P2 single mutant C213A, and double mutant F8A/C213A were made by following the QuickChange mutagenesis protocol using whole-plasmid polymerase chain reaction (PCR). CheY single-cysteine mutants (E89C, and K91C) were made by following the overlap extension PCR protocol. The P1 Δ9 (residues 10−134) mutant was made by following the regular PCR protocol. *Pfu Turbo* DNA polymerase (Stratagene) was used for all PCRs. Restriction enzymes and T4 DNA ligase were purchased from New England Biolabs. All mutations were confirmed by DNA sequencing and expressed and purified with the same protocols that were used for the wild-type proteins.

Site-Directed Spin Labeling of CheY. CheY cysteine mutants in 50 mM sodium phosphate and 150 mM sodium chloride (pH 7.9) were treated with 5 mM dithiothreitol (DTT) for 1 h to prevent the dimerization 1 h prior to spin labeling. DTT was removed with a Sephadex G-25 (Sigma) spin column immediately before the modification with MTSL [(1-oxyl-2,2,5,5-tetramethylpyrroline-3-methyl)-methanethiosulfonate], in which the nitroxide spin-label was attached to the single cysteine through a disulfide bond;[13] 1−2% (v/v) of the concentrated MTSL stock in ethanol was added to the sample at a 10:1 MTSL:protein molar ratio and incubated at room temperature for 2 h, and the G-25 spin

dx.doi.org/10.1021/bi300147m | *Biochemistry* 2012, 51, 3786−3798

column was used to remove the excess free MTSL and exchange the sample into NMR buffer [50 mM sodium phosphate (pH 6.5)]. The color test developed by Murray et al.[18] was used to ensure the completion of the MTSL modification. The modified protein was concentrated and used at 100 μM for NMR experiments. The modified CheY mutant was mixed with 100 μM deuterated P1P2 C213A, and a $^{1}H-^{15}N$ heteronuclear single-quantum coherence (HSQC) spectrum was recorded.[19] As a reference, another $^{1}H-^{15}N$ HSQC spectrum was recorded after the MTSL in the sample was reduced by the incubation with a 200-fold excess of ascorbic acid at room temperature in the dark for at least 10 h.[13,14] Control experiments were performed using the same method, but with P1P2 F8A/C213A instead of P1P2 C213A.

NMR Spectroscopy. All the data reported in this study were collected with a Varian Inova 600 MHz spectrometer equipped with a cryoprobe at 25 °C. NMR data were analyzed with the nmrPipe package, and assignments were made with ANSIG3.3.[20,21] All NMR samples (except for those for spin-label experiments) were in 50 mM sodium phosphate (pH 6.5). DTT (5 mM), sodium azide (0.2%), and D_2O (8%) were added prior to NMR experiments. Samples used in experiments requiring D_2O-based buffers were lyophilized after dialysis and dissolved in 99.8% D_2O.

The backbone and side chain sequential assignments were obtained from the following two- and three-dimensional experiments: $^{1}H-^{15}N$ HSQC,[19] $^{1}H-^{13}C$ HSQC,[22] HNCACB,[23] HNCO,[18,23] (H)C(CO)NH-TOCSY,[24−26] and H(C)(CO)NH-TOCSY.[24−26]

The P1−CheY−P2 complex chemical shift assignments were made by tracing the complex resonances through titration experiments back to the resonances of their unbound states. Titration experiments were conducted with the following samples: 200 μM [^{15}N,^{2}H]P1 was titrated with the mixture of 3 mM unlabeled CheY and 3.2 mM [^{2}H]P2; 200 μM [^{15}N,^{2}H]CheY and 250 μM [^{2}H]P2 were titrated with 3 mM [^{2}H]P1.

Additionally, multidimensional nuclear Overhauser effect spectroscopy (NOESY) spectra[27] were recorded for interproton distance restraints: three-dimensional ^{13}C-separated/^{12}C-filtered NOESY using a ^{1}H-, ^{15}N-, and ^{13}C-labeled sample (3 mM CheY or P1) and its respective unlabeled partner in D_2O buffer and four-dimensional ^{15}N,^{13}C-edited NOESY using a ^{2}H- and ^{15}N-labeled sample (3 mM CheY or P1) and its respective ^{2}H- and ^{13}C-labeled partner in H_2O buffer.[28] A ^{2}H-, ^{14}N-, and ^{12}C-labeled P2 sample (2 or 3 mM) was used in all of these experiments.

Calculation of K_d. To estimate the affinity of the P1−CheY complex, we monitored the extent of the interaction by the chemical shift perturbation of the representative residues of ^{15}N-labeled proteins as a function of the concentration of their interaction partner.[29] The resulting data points (CSP, chemical shift perturbation) were fit with a model that consists of the product of the chemical shift perturbation for a given residue at the saturation point (CSP_{max}) and the fraction of the bound species (f_{bound}), with the dissociation constant (K_d) and CSP_{max} as adjustable parameters:

$$CSP = CSP_{max} \times f_{bound}$$

The fraction of the bound species was expressed as follows (in cases where P1 is the titrant):

$$f_{bound}[P1] = \frac{1}{2}\left(\frac{K_d + [P1]}{[CheY_{total}]} + 1\right) - \frac{1}{2} \times \sqrt{\left(\frac{K_d + [P1]}{[CheY_{total}]} + 1\right)^2 - 4\frac{[P1]}{[CheY_{total}]}}$$

Structure Calculation. Distance constraints derived from the intermolecular NOE experiments were conservatively classified into three levels, 1.8−4.2, 1.8−5.2, and 1.8−7.2 Å, corresponding to strong, medium, and weak NOEs, respectively. Long-range distance constraints were derived from the site-directed spin labeling experiment. On the basis of the ratio of the intensity of the oxidized protein spectrum to that of the reduced protein spectrum (I_{ox}/I_{red}), the distance constraint of 1.8−15 Å was assigned for the peaks that were broadened more than 35%.[30−38]

The starting structures were generated by linking the P2 domain of the *E. coli* CheY−P2 complex [Protein Data Bank (PDB) entry 1EAY] to the structure of the *Salmonella typhimurium* P1 domain (PDB entry 1I5N) by the *E. coli* linker sequence, because the structure of *E. coli* P1 is not available.[15,39] Residues 1−3 and 132−134, which are not visible in 1I5N, were also added. The level of sequence identity between *S. typhimurium* and *E. coli* P1 (residues 1−134) is 94%, and all nuclei for which we observed NOEs belonged to residues that were identical in both proteins. Residues 60 and 61, for which we observed the paramagnetic broadening in the spin-label experiment, are not identical, but they were backbone amides and therefore deemed equivalent in both proteins; 200 of such structures were generated starting from random initial orientations and separations, and four rounds of refinement were conducted using the 26 NOE constraints and 14 spin-label constraints listed in Table 2. The simulated annealing protocol of XPLOR-NIH was used to calculate the structures.[40] The P1 and CheY−P2 complex were docked as rigid bodies, with the following exceptions: the side chains of residues responsible for the interaction based on NOEs and the chemical shift perturbation were allowed to move freely in the torsion angle dynamics simulation (P1 residues 1−20 and 50−60 and CheY residues 9−26, 57−59, 86−91, and 111−114). Both the side chains and backbone of the first three and last three residues of P1, whose coordinates were not shown in the crystal structure probably because of the flexibility of the termini, the 23-residue linker between P1 and P2, and residues surrounding these regions (CheA residues 1−7 and 132−159) were also allowed to move.

Stopped-Flow Observation of CheY W58 Fluorescence. Activation of the P1 domain by transphosphorylation was done by incubating 100 μM ^{15}N-labeled P1 with 10 μM CheA P3P4P5 (residues 261−654) and 10 mM ATP in 50 mM Tris-HCl, 5 mM $MgCl_2$, 100 mM KCl, and 0.5 mM DTT (pH 8.2) for >4 h. $^{1}H-^{15}N$ HSQC experiments were used to assess the extent of phosphorylation.[41]

The time course for CheY phosphorylation was monitored by the decrease in the intrinsic tryptophan fluorescence of CheY.[7] CheY was mixed with various phosphorylated P1 constructs in a stopped-flow spectrofluorometer (Applied Photophysics SX.18MV, dead time of ∼2 ms). The reaction mixtures were kept at 24−25 °C in the observation chamber of the instrument with a thermostat; the samples were excited at 295 nm (∼7 nm slit width on the excitation monochromator), and fluorescence emission was monitored at a combination of

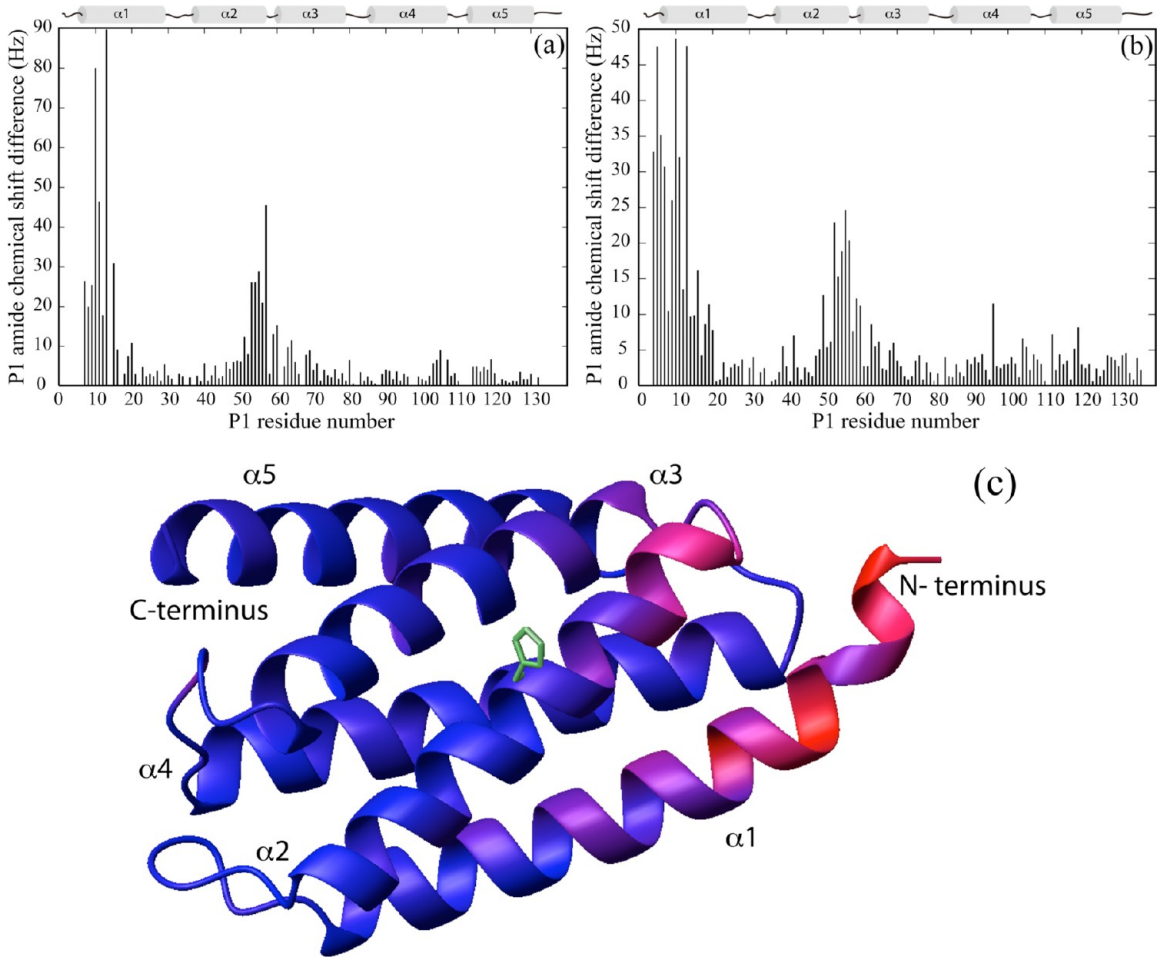

Figure 2. (a) Chemical shift perturbation of the P1 domain by CheY. ^{15}N-labeled P1 (200 μM) was titrated with 2 mM unlabeled CheY, and the chemical shift difference, $[(\Delta\delta^{1}\mathrm{H} \times 600)^2 + (\Delta\delta^{15}\mathrm{N} \times 60.8)^2]^{1/2}$, at the titration end point for each P1 residue was plotted. (b) Chemical shift perturbation of the P1 domain by CheY complexed with the P2 domain. ^{15}N-labeled P1 (200 μM) was titrated with 3 mM deuterated, unlabeled CheY and P2, and the resulting chemical shift difference for each P1 residue was plotted. (c) Chemical shift perturbation in the presence of CheY shown in panel b color-coded and plotted onto the P1 structure (PDB entry 1I5N). Red indicates larger chemical shift differences. Residues colored blue exhibited smaller differences. The active site histidine and its side chain are colored green.

wavelengths above 320 nm with a cutoff filter. All phosphotransfer reactions were conducted in 50 mM Tris-HCl, 5 mM $MgCl_2$, and 0.5 mM DTT (pH 7.5).[42]

Data were fit to the following kinetic scheme:

$$\mathrm{A{-}P} + \mathrm{Y} \xrightarrow{k_1} \underset{+\ \mathrm{A}}{\mathrm{Y{-}P}} \xrightarrow{k_2} \mathrm{Y} + \mathrm{P}$$

where A−P is the phosphorylated form of the P1 domain of CheA, Y is CheY, and Y−P is the phosphorylated form of CheY. Phosphorylation of CheY results in a decrease in tryptophan fluorescence. In the presence of excess CheY, the phosphorylation time course as observed from the CheY perspective can be described as the disappearance of free CheY fluorescence due to phosphorylation followed by its recovery due to autodephosphorylation:

$$\mathrm{Y} \xrightarrow{k_1[\mathrm{Y}]} \mathrm{Y{-}P} \xrightarrow{k_2} \mathrm{Y}$$

where the phosphotransfer step becomes pseudo-first-order and equal to the product k_1[CheY], where k_1 is the apparent second-order rate constant for phosphotransfer from P1 to CheY. The change in CheY fluorescence $F(t)$ as a function of time is then

$$F(t) = c + a(\mathrm{e}^{-bt} - \mathrm{e}^{-dt})$$

where c is the fluorescence at time zero, $d = k_2$, $b = k_1$[CheY], and $a = F_{\mathrm{CheY\text{-}P}}A_0k_1[\mathrm{CheY}]/(k_2 - k_1[\mathrm{CheY}])$, where $F_{\mathrm{CheY\text{-}P}}$ represents the fluorescence of fully phosphorylated CheY and A_0 is the initial concentration of phosphorylated P1.[43]

RESULTS

CheA P1 Interacts with CheY Weakly yet Specifically. To identify the residues of CheA P1 responsible for its interaction with CheY, we titrated ^{15}N-labeled P1 with unlabeled CheY. The extent of interaction was monitored by the ^{1}H−^{15}N HSQC spectrum of P1, and the residues with significant chemical shift perturbations were mapped onto the structure of P1 (Figure 2a,c). The P1 residues that showed the largest chemical shift perturbation were residues 4−20 (the beginning of α1) and residues 50 and 53−60 (the end of α2 and the turn that connects it to α3), which together form a continuous surface on the P1 structure. These results suggest that there is one specific CheY-binding surface on the P1 domain.

Chemical shift perturbations of ^{15}N-labeled CheY by unlabeled P1, on the other hand, showed that there were two

dx.doi.org/10.1021/bi300147m | Biochemistry 2012, 51, 3786−3798

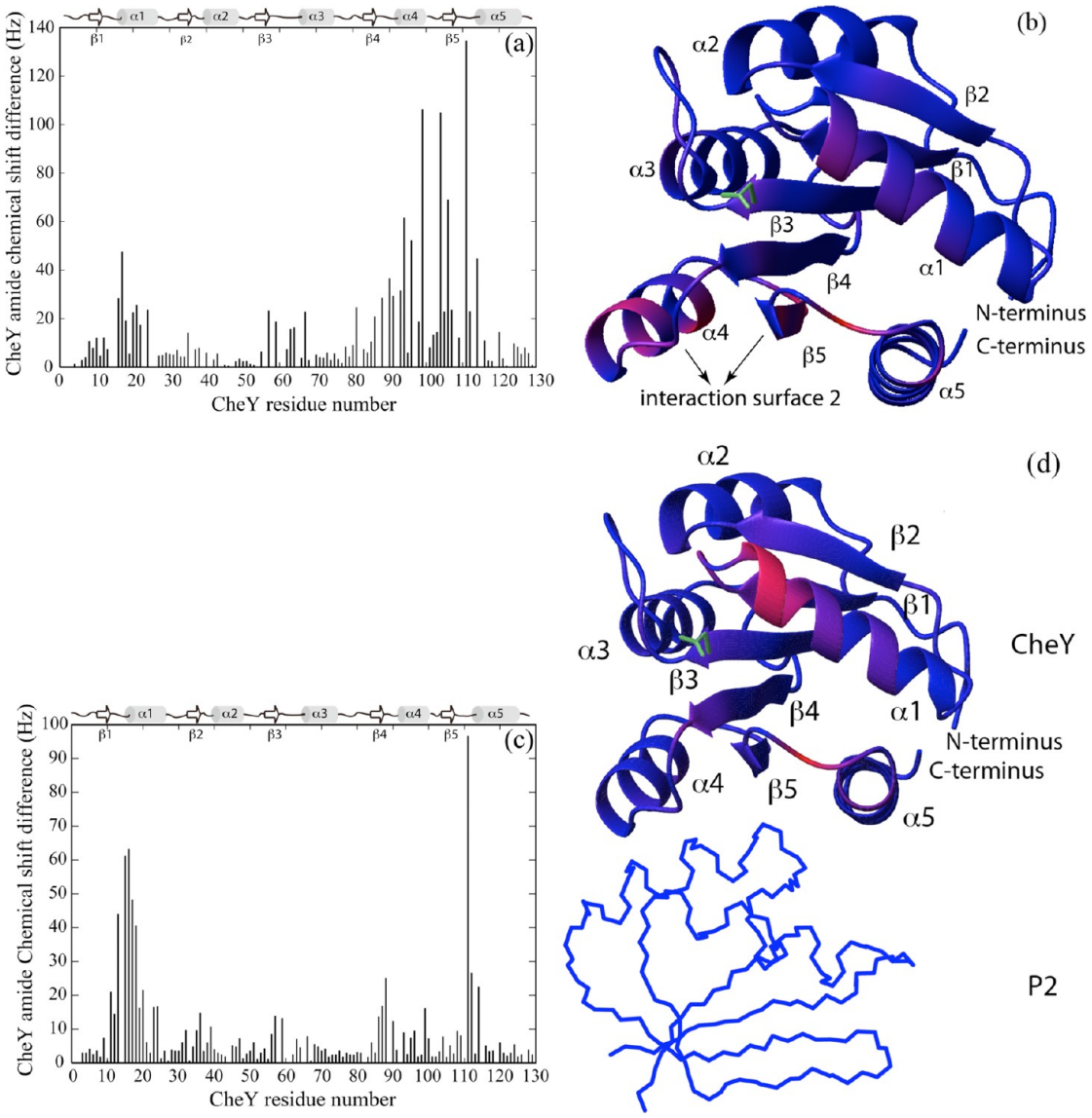

Figure 3. (a) Chemical shift perturbation of CheY by the P1 domain. ^{15}N-labeled CheY (200 μM) was titrated with 2.4 mM unlabeled P1, and the chemical shift difference at the titration end point for each CheY residue was plotted. (b) Chemical shift perturbation in the presence of P1 shown in panel a color-coded and plotted on the CheY structure (PDB entry 3CHY). Red indicates larger chemical shift differences. Residues colored blue exhibited smaller differences. The active site aspartate and its side chain are colored green. (c) Chemical shift perturbation of CheY complexed with the P2 domain by P1. ^{15}N-labeled CheY (200 μM) complexed with deuterated, unlabeled P2 was titrated with 2.4 mM deuterated, unlabeled P1, and the chemical shift difference at the titration end point for each CheY residue was plotted. (d) Chemical shift perturbation of CheY complexed with P2 (PDB entry 1EAY) in the presence of P1 shown in panel c color-coded and plotted on the CheY structure. Red indicates larger chemical shift differences. Residues colored blue exhibited smaller differences. The active site aspartate and its side chain are colored green.

separate surfaces on CheY that interact with P1 (Figure 3a,b). The first interaction surface is centered around the active site Asp 57. The second surface overlapped the interface between CheY and the CheA P2 domain as evidenced by the crystal structure of the CheY−P2 complex.[15,44,45] CheY is known to bind to P2 with a dissociation constant (K_d) in the low micromolar range, which is much weaker than the K_d for the P1−CheY interaction (see below). We asked if the second mode of interaction between CheY and P1 could be eliminated if the experiment was repeated in the presence of a saturating amount of P2.[45,46] Not surprisingly, when high levels of P2 were present, the CheY residues involved in the interaction with P2, which comprise the majority of the second P1 interaction surface, did not exhibit significant chemical shift changes upon addition of P1, and the P1 interaction was now limited to the surface surrounding the site of phosphotransfer (Figure 3c,d). This indicates the second mode of interaction observed in the absence of P2 was likely a nonproductive one. The CheY residues showing the largest chemical shift perturbations by P1 included residues 9−20 (the turn following β1 and the beginning of α1), residues 57−59 (the end of β3, the active site), residues 86−90 (the end of β4 and the turn leading to α4), and residues 111−114 (the turn following β5 and the beginning of α5). This is largely consistent with the mode of interaction seen in the crystal structures of the yeast Ypd1−SLN1 (R1) complex and the $CheA_3P1-CheY_6$ complex of *R. sphaeroides* discussed above.[11,12]

On the basis of the concentration dependence of the chemical shift perturbation, we estimated the dissociation constant, K_d, between the P1 domain and CheY in the presence

dx.doi.org/10.1021/bi300147m | *Biochemistry* 2012, 51, 3786−3798

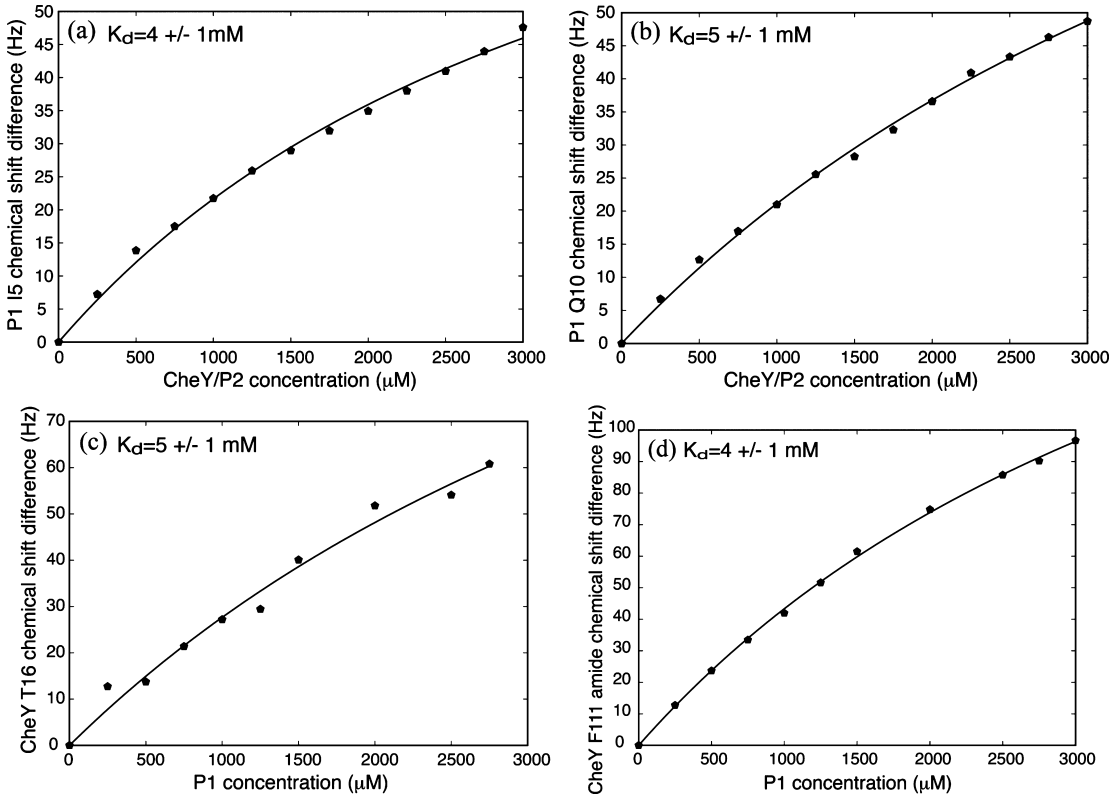

Figure 4. Affinity of the P1−CheY interaction. For both P1 (a and b) and CheY (c and d), titration curves were constructed for representative residues by monitoring their amide chemical shift perturbations throughout the course of the titrations shown in Figures 2 and 3 and fitting them with a model described in Materials and Methods. The dissociation constant was estimated by taking their average value (~4.5 mM).

of the unlinked P2 domain to be ~5 mM (Figure 4). Also, the presence of P2 did not seem to affect the CheY−interaction surface of P1, as the residues that exhibited the largest chemical shift perturbation were mostly the same with or without P2 (Figure 2b,c). Taken together, these results suggest there is a weak but specific mode of interaction between CheY and P1 in the presence of P2, even when the linker between P1 and P2 is absent.

The Observed Interaction between P1 and the CheY−P2 Complex Is Biochemically Relevant. Our results indicate that only a small number of residues are involved in the P1−CheY interaction and that the affinity is very weak. We wondered whether the interaction we detected was the one that leads to phosphorylation. To address this question, we mutated selected P1 residues within the proposed binding surface and examined their effects on the rate of phosphotransfer from P1 to CheY by monitoring the fluorescence quenching of CheY W58 upon phosphorylation of D57.[42] All mutants are folded correctly as confirmed by ^{15}N HSQC spectra (data not shown). Mutation of P1 residues F8 and E15 to alanine dramatically weakened its interaction with the CheY−P2 complex, as evidenced by the lack of chemical shift perturbation, and deletion of the first nine residues of the N-terminus of P1 also nearly abolished the interaction (data not shown). The phosphotransfer rate was 5−30 times slower for these mutants than for wild-type P1 (Figure 5 and Table 1). In total, we introduced eight separate mutations into the proposed binding surface of P1, but we were unable to isolate a mutant whose binding was compromised but phosphotransfer rate was not. These results suggest that the mode of interaction between P1 and CheY we detected is the one that leads to phosphotransfer.

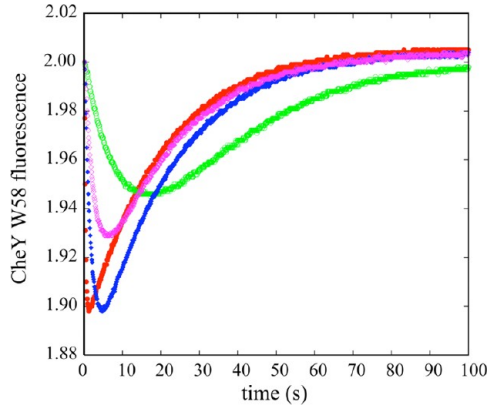

Figure 5. Time course of CheY phosphorylation monitored by CheY W58 fluorescence quenching. The fluorescence emission intensity of 1 μM CheY was monitored as it was mixed with various P1 constructs at 0.25 μM (red for wild-type P1, blue for P1 F8A, magenta for P1 E15A, and green for P1 Δ9), which had been activated prior to mixing. For each P1 construct, the measurement was repeated at least three times, and the data were averaged. The initial value for CheY fluorescence for each time course was normalized for comparison. Results for the first 100 s are shown.

NOE-Based Short-Range Distance Constraints. Having seen that the observed P1−CheY interaction was biochemically relevant, we proceeded to construct a structural model for this interaction. Multidimensional NOESY was used to provide the short-range distance constraints between the P1 domain and CheY complexed with the P2 domain. The unlinked P2 was used to eliminate the nonspecific interaction between P1 and

dx.doi.org/10.1021/bi300147m | *Biochemistry* 2012, 51, 3786−3798

Table 1. Kinetic Parameters for Phosphotransfer by PI Mutants

construct	k_{phos} (M^{-1} s^{-1})	k_{dephos} (s^{-1})
wild-type P1	2.5×10^6	0.050
P1 Δ9	0.075×10^6	0.046
P1 F8A	0.55×10^6	0.050
P1 E15A	0.36×10^6	0.049

CheY discussed above. Examples of the resulting NOESY spectra are shown in panels a and b of Figure 6, and the residues responsible for the intermolecular NOEs are mapped onto P1 and CheY structures (Figure 7b,c). In total, 26 intermolecular NOEs between 11 P1 residues and 9 residues of CheY were observed (Table 2). Residues 3, 5, 8, 11−16, and 56 of P1 gave intermolecular NOEs, and most of them are located at the N-terminus of α1. Residues 16, 18−20, 23, 24, 109, and 111 of CheY contributed to the intermolecular NOEs. These residues are located at the N-terminus of α1, and in the loop connecting β5 and α5. The results from the NOE experiment and the chemical shift perturbation results of the ^{15}N HSQC titration experiments are in excellent agreement.

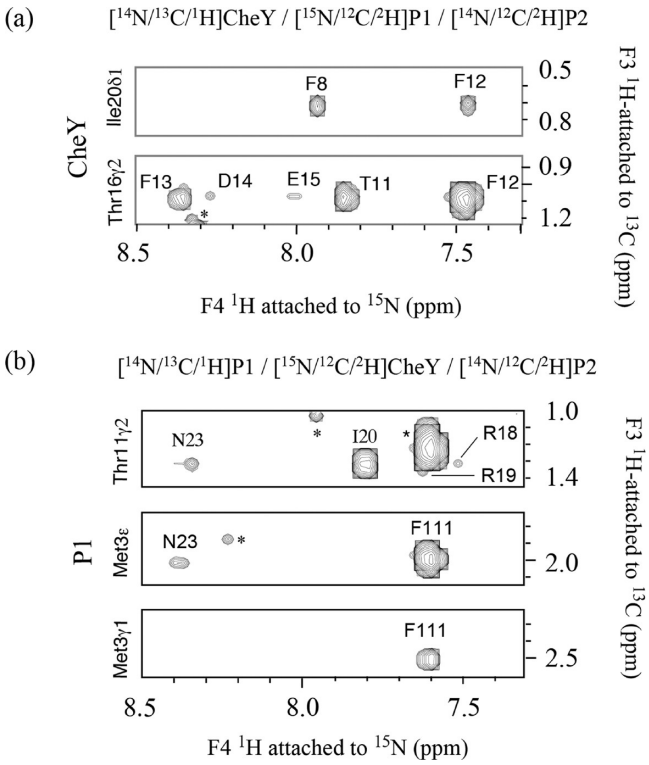

Figure 6. Observed NOEs between P1 and CheY in the P1−CheY−P2 complex. NOEs were obtained from four-dimensional ^{15}N,^{13}C-edited NOE experiments that provide the intermolecular NOE between protons attached to ^{15}N on one protein and protons attached to ^{13}C on the other protein. The P2 domain is deuterated and unlabeled in both cases. In the experiments shown in panel a, CheY is ^{13}C-labeled and P1 is ^{15}N-labeled and deuterated. The top panel shows the plane at 13.7 ppm in ^{13}C and 121 ppm in ^{15}N, which shows the NOEs between the CheY I20 δ1 methyl protons and P1 F12 and F8 backbone amide protons. The bottom panel shows the NOEs from CheY T16 γ2 methyl protons to several P1 amides on the plane at 22.1 ppm in ^{13}C and 118 ppm in ^{15}N. In panel b, the P1 domain is ^{13}C-labeled and CheY is deuterated and ^{15}N-labeled. The top panel shows the plane at 22.3 ppm in ^{13}C and 118 ppm in ^{15}N, which shows the NOEs between the P1 T11 δ2 methyl protons and CheY R18, R19, I20, and N23 backbone amide protons. The middle panel shows the NOEs from P1M3 ε methyl protons to CheY N23 and F111 amides on the plane at 17.6 ppm in ^{13}C and 119 ppm in ^{15}N. The bottom panel shows the NOEs from P1M3 γ1 methyl protons to P1 F111 amides on the plane at 32.2 ppm in ^{13}C and 116 ppm in ^{15}N.

Long-Range Distance Constraints Based on Site-Directed Spin Labeling. Results of the titration and NOESY experiments showed that P1 and CheY residues responsible for the direct interaction were clustered into a small region in both proteins. To supplement the NOE-based short-range distance information during the structure calculation, we used site-directed spin labeling to obtain long-range distance constraints from the parts of the proteins that did not have NOEs.

Two single-cysteine mutants of CheY were constructed for site-directed nitroxide spin labeling with MTSL (Table 2). The positions of the mutation (residues 89 and 91) were chosen to be close to the active site Asp 57 and far from the binding interface determined by the chemical shift perturbation mapping and NOEs (Figure 7b,c). These mutations are in loops and exposed to the solvent and not expected to disrupt the three-dimensional structure of CheY. The ^{1}H−^{15}N HSQC spectra of these mutants showed only minor chemical shift perturbations around the sites of mutations, suggesting their effects on the global structure are negligible. Also, the mutations did not seem to affect the interaction with the P1 domain, as the chemical shift perturbations in the ^{1}H−^{15}N HSQC spectra of P1 bound to these mutants were indistinguishable from those caused by the wild-type protein (data not shown).

To identify the P1 residues in the proximity of the spin labeling sites, each CheY mutant labeled with MTSL was mixed with the P1P2 construct of CheA (residues 1−233, the P1 domain, and the P2 domain connected with the native linker), a ^{1}H−^{15}N HSQC spectrum was collected, and the resulting resonance intensity for each P1P2 backbone amide ($I_{oxidized}$) was recorded. To quantify the paramagnetic broadening of the resonances, we repeated the same experiment after the MTSL in the sample was inactivated by the addition of excess ascorbic acid to yield the baseline value ($I_{reduced}$). To eliminate the effects of possible nonspecific interactions, we performed a control experiment for each CheY mutant by using P1P2 F8A, a P1P2 mutant with reduced affinity for CheY. We reasoned that nonspecific interactions were unlikely to be changed by this mutation but the specific interactions should be significantly weakened.

Figure 7a shows the resulting peak intensity ratio ($I_{oxidized}$/$I_{reduced}$) plotted against the P1 residue numbers when the P1P2 fragment was mixed with the CheY mutant labeled with MTSL at residue 89. It indicates P1 amide resonances broadened by MTSL at this position were those of residues 8, 9, 12, 52, 53, 55, 57−68, 82, 85, 108, and 126. Among them, residue 12 and residues 85 and 108 and their adjacent residues were also shown to be broadened in the control experiment with P1P2 F8A. The results for these residues were not used as distance constraints in the structure calculation (Figure 7b). P1 residues affected by CheY K91C labeled with MTSL at different positions were also identified likewise (Table 2). These results provided additional information about the distance between the second and third helices of P1 and the active site surface of CheY.

dx.doi.org/10.1021/bi300147m | *Biochemistry* 2012, 51, 3786−3798

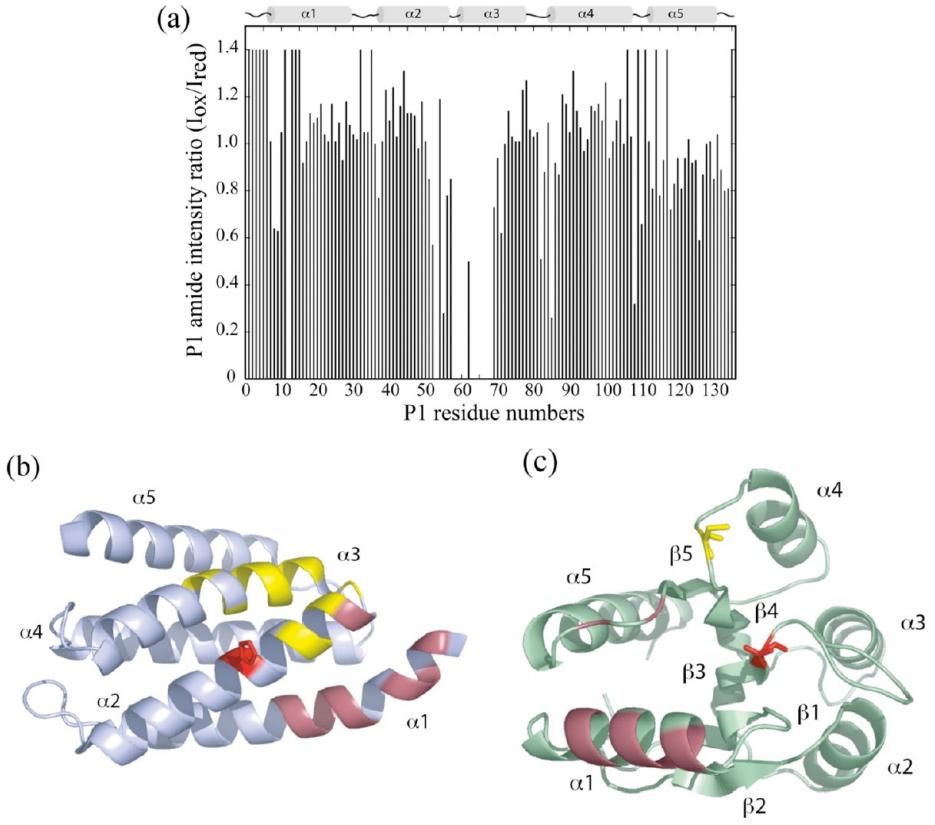

Figure 7. (a) Paramagnetic broadening of P1 amide resonances by CheY mutants spin-labeled with MTSL. The ^{15}N-labeled P1P2 fragment was mixed with CheY constructs labeled with MTSL at various positions, including E89C used in the experiment shown here. The ratio of P1 amide intensity to oxidized (active) and reduced (inactive) spin-label was plotted across the P1 sequence. An arbitrary intensity ratio of 1.40 was assigned to residues for which the intensity ratio could not be calculated because of resonance overlap or a lack of assignment. Assignments of the distance restraints as well as the results obtained with CheY constructs containing the spin-labels at other positions are summarized in Table 2. (b and c) Observed intermolecular NOEs listed in Table 2 are colored dark red and plotted on the structures of P1 (b) and CheY (c). The paramagnetic broadening of P1 amide resonances by CheY E89C is colored yellow (b). The location of the spin-label at position 89 is colored yellow (c). The active site histidine and aspartate and their side chains are colored red.

Structural Model for the P1P2−CheY Complex. The crystal structures of the isolated P1 domain (PDB entry 1I5N), the P2 domain (PDB entry 1FWP), CheY (PDB entry 3CHY), and the CheY−P2 complex (PDB entry 1EAY) have been determined previously.[15,39,47,48] To initiate model building for the P1P2−CheY complex, we generated a starting structure, in which the structure of P1 was connected by the native linker to P2 in the CheY−P2 complex structure. Two hundred such structures were refined by four successive rounds of simulated annealing and torsion angle dynamics, using the distance constraints obtained from the NOE experiments and the spin-label experiments with MTSL. The NOE-based distance constraints were classified into three levels, 1.8−4.2, 1.8−5.2, and 1.8−7.2 Å, corresponding to strong, medium, and weak NOEs, respectively. The MTSL-based longer distance constraints were assigned to 1.8−15 Å for the peaks that were broadened more than 35%, based on the ratio of the intensity of the oxidized spectrum to that of the reduced spectrum ($I_{oxidized}/I_{reduced}$). During the refinement, the flexible N-terminal residues of P1, the residues in the P1−P2 linker region, and the side chains of the residues responsible for the interactions as determined by NOE and chemical shift perturbation (see Materials and Methods) were allowed to move freely in the torsion angle space; otherwise, each domain was treated as a rigid body, for the chemical shift perturbation in our titration experiments suggested that there were small global structural changes.

Superposition of the 50 lowest-energy structures with no distance violation is shown in Figure 8a. The P1 backbone root-

Table 2. Summary of the Observed Intermolecular NOE and Long-Range Distance Constraints[a] Obtained from MTSL Experiments

CheY nucleus	P1 nuclei
T16 $H_\gamma 2^b$	T11 HN, F12 HN, F13 HN, D14 HN, E15 HN, A16 HN
R18 HN	T11 $H_\gamma 2^b$
R19 H_β^b	T11 $H_\gamma 2$,[b] E15 HN
R19 HN	T11 $H_\gamma 2^b$
120 $H_\delta 1^b$	M3 H_ε,[b] F8 HN, T11 $H_\gamma 2$,[b] F12 HN, T56 $H_\gamma 2^b$
120 HN	T11 $H_\gamma 2^b$
N23 H_δ^b	T11 $H_\gamma 2^b$
N23 HN	M3 $H_{g'}^b$ T11 $H_\gamma 2^b$
L24 HN	M3 H_ε^b
K109 HN	M3 H_ε^b
F111 HN	M3 $H_\beta 1$, M3 $H_\gamma 1$, M3 $H_{g'}$,[b] 15 $H_\gamma 2$,[b] 15 H_δ^b
MTSL position on CheY	**P1 residues broadened by MTSL**
E89C	52HN, 53HN, 55HN, 58HN, 60−66HN, 68HN
K91C	Q63 H_ε,[b] N71 H_δ^b

[a]Only the results used in the structure calculation are shown here. [b]Three equivalent protons on methyl groups.

dx.doi.org/10.1021/bi300147m | *Biochemistry* 2012, 51, 3786−3798

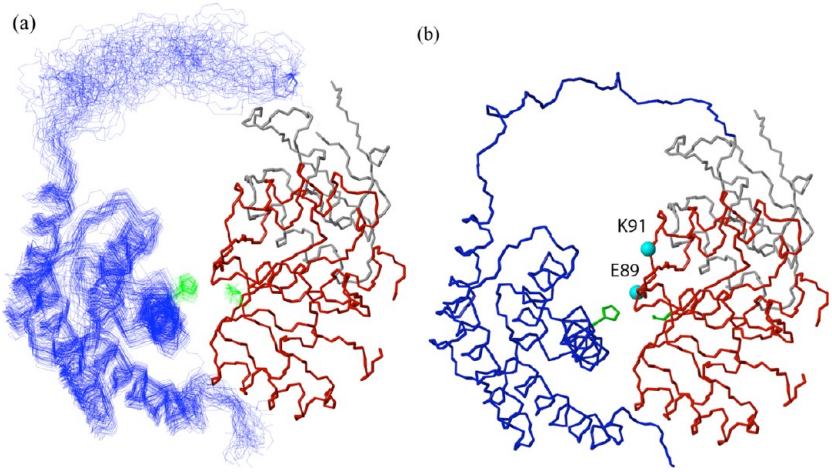

Figure 8. Structural model for the P1P2−CheY complex in solution. (a) Superposition of the 50 lowest-energy results from the calculation with no distance constraint violation. The backbone rmsd for the P1 domain in this bundle, when the backbone of the CheY−P2 complex was aligned, was 1.3 Å. The average C_α−C_α distance between the active site H48 and D57 is 11.7 Å. The average distances between H48 N_ϵ and D57 O1 and O2 are 5.91 and 5.52 Å, respectively. (b) Representative of 50 bundles shown in panel a. P1 and the linker are colored blue; CheY is colored red, and P2 is colored gray. The active site side chains are colored green. Spin-labeled positions E89 and K91 are denoted.

mean-square deviation (rmsd) was ∼1.3 Å when the backbone of the CheY−P2 complex was aligned. Residues responsible for interactions that collectively hold these two domains in the observed orientation are confined in seemingly small regions. The CheY−interaction surface of P1 appears to be located mainly in the first half of α1 and the end of α2. On the CheY side, the interacting residues are mostly in its α1 and the adjacent loop between β5 and α5. Figure 10a shows a detailed view of the interface between these two regions. A thread of interaction takes place as two faces of CheY α1 (T16-I20-L24 and R19-N23) interlock with the side chains of the D7-F8-T11-E15 face of P1 α1. Additionally, P1 I5 (on a different face of α1) and M3 (in the N-terminal loop) interact with two CheY residues (F111 and K109) in the β5−α5 loop, which completes the trapezoidal plane of an interacting surface. The interaction between P1 T56 (at the end of α2) and CheY I20 should provide another source of stability to the complex.

This small web of interactions leads to such a degree of convergence among the calculated results that the C_α−C_α distance between the active site of P1 and CheY ranges from 11.3 to 12.3 Å for the 50 structures (Figure 8a). This proximity alone should make phosphorylation of CheY by P1 much more favorable than phosphorylation by small molecule phosphodonors with no specific affinity for CheY. The distance between the C-terminus of the P1 domain (residue 131) and the N-terminus of the P2 domain (residue 160) was approximately 45 Å, which is expected from a flexible linker of this length (see Discussion).

DISCUSSION

In this study, we constructed a structural model for the interaction of the *E. coli* chemotactic proteins CheY and CheA P1, in the presence of the CheY-binding domain of CheA, P2. Although complex structures of their homologues (*R. sphaeroides* $CheA_3P1$−$CheY_6$) and the structural homologues (yeast Ypd1−Sln1) have been reported, these systems differ from the *E. coli* system in that they lack the additional domain dedicated to binding to the response regulator, and the interaction of a histidine phosphate transfer domain (HPt) with a response regulator domain (RR) in the presence of such a domain has not been examined on a structural basis. Here we discuss the overall evaluation of the resulting model, its relation to the previously reported structures of the HPt−RR complexes, and its biological significance.

Evaluation of the P1−CheY−P2 Complex Structure. In our structural calculation, CheY and P1 were treated as rigid bodies and docked on the basis of the distance information gained from the NOESY experiments and site-directed spin-label experiments with MTSL. Our approach to model building, based on the distance information alone, is an abbreviated version of the procedure pioneered by the Clore group in their work on the sugar transport systems.[30−38] The backbone rmsd for the P1 domain in the final 50 lowest-energy structures, when the backbone of the CheY−P2 complex was held constant, was ∼1.3 Å (Figure 8). This degree of convergence is significantly lower compared to the standard set by the work of the Clore group, which typically includes the torsion angle constraints and constraints derived from the residual dipolar coupling, in addition to the NOE-based distant constraints, with the reported convergence rates ranging from 0.1 Å for the mannitol transporter system to 0.5 Å for the mannose transporter system.[30−38] Our approach is based only on the conservative distance constraints, lacks residual dipolar coupling data, and as a result does not match the apparent resolution reported by the Clore group. The lower resolution in our work represents a valid alternative in addressing issues when lower-resolution structural information answers the questions at hand with a significantly smaller investment in machine and data analysis time.

The low degree of convergence in the P1−CheY model is also due to the fact that the interaction appears to be mediated by a single, small surface on both proteins. Our NOE results show that the major interaction is mediated by a plane defined by part of a helix (residues 14−24) and a few residues in the adjacent loop (residues 109−112) in CheY, and only a handful of P1 residues, mostly in its N-terminal loop and α1, make contact with these residues. The importance of the P1 residues lining the proposed interface was confirmed by our observation that an alanine mutation at many of these positions severely compromises the interaction, and this seems to indicate that

dx.doi.org/10.1021/bi300147m | *Biochemistry* 2012, 51, 3786−3798

this surface is largely, perhaps solely, responsible for the interaction. The interactions between P1 and CheY, as outlined above, contained enough information to align the side chains of the two active site residues, P1 H48 and CheY D57, at a short distance. In a majority of the 50 calculated structures, the distance from catalytic H48 $H_\varepsilon 2$ of P1 to D57 $O_\delta 1/2$ of CheY was between 4 and 7 Å (Figure 8). P1 is known to phosphorylate CheY a few thousand-fold faster than the small-molecule phosphate donors at comparable concentrations, presumably because of the participation of its active site residues.[7]

Comparison of the P1−CheY Model with the Previously Reported Structures of the HPt−RR Complex. A few high-resolution HK−RR complex crystal structures have been determined previously: the Spo0B−Sp0F complex in the *Bacillus subtilis* sporulation regulation system, the hypothetical HPt−RR combination, HK853−RR468, in *Thermotoga maritima*, the Ypd1−SLN1 (R1) complex in the yeast environmental stress response system, and the $CheA_3P1$−$CheY_6$ complex in the *R. sphaeroides* chemotaxis two-component system.[9−12,49,50] While the structures of the RR domains are highly conserved, the structural feature of the HPt domains is loosely defined as a helix bundle with the active site histidine that interacts with the active site aspartate of the CheY-like response regulators; its members are not always structural homologues, and their sequences are often not conserved beyond the small regions around the catalytic histidine.[41] The domain architecture of Spo0B and HK835 cP is a dimer of two-helix bundles with the active site histidine in each monomer, and these are not homologous to *E. coli* P1.[9,10] On the other hand, yeast Ypd1 is a monomeric HPt protein that has a four-helix bundle with an additional short helix at the N-terminus and is a structural homologue of P1.[11] Also, $CheA_3P1$ is a five-helix bundle monomeric HPt protein and one of the three *R. sphaeroides* orthologs of *E. coli* CheA P1.[12] We compared these two structures with our model, and the results showed that, while *E. coli* P1 and CheY employ a mode of interaction similar to those seen in these structures, the presence of P2 and the linker might lead to a slightly different orientation of the HPt domain with respect to the RR domain (Figure 9).

In all three cases, two major factors stabilizing the complex appear to be (1) the interaction between α-helix 1 of the RR domain and the helices equivalent to α-helix 1 of *E. coli* P1 and (2) the interaction of the helix containing the active site histidine of the HPt domain with the $\beta 5$−$\alpha 5$ loop of the RR.[11,12] However, the resulting relative orientation of the HPt domain with respect to the RR domain is slightly different. When the CheY and $CheY_6$ parts are held constant (alignment rmsd of ∼1.18 Å), *E. coli* P1 is rotated (by ∼30°) with respect to *R. sphaeroides* $CheA_3P1$ such that the part of the P1 interaction surface of CheY close to its P2 interface is more exposed in the *E. coli* model (Figure 9). The orientation of the HPt domain with respect to the RR domain in the yeast Ypd1−SLN1(R1) complex is similar to that in the *R. sphaeroides* complex. The average C_α−C_α distance between the active sites in *E. coli* structures is within the range of the two other systems (11.7 Å in *E. coli*, 14 Å in *R. sphaeroides*, and 10.2 Å in yeast), as well as their average catalytic side chain atoms (H48 $N_\varepsilon 2$ to D57 $O_\delta 1$ and $O_\delta 2$, 5.9 and 5.5 Å in *E. coli*, 7.3 and 7.04 Å in *R. sphaeroides*, and 4.58 and 3.91 Å in yeast, respectively).[12]

What is the meaning of such differences? There are reasons to think that our results might represent a biologically relevant species. A recent statistical analysis indicates that pairs of

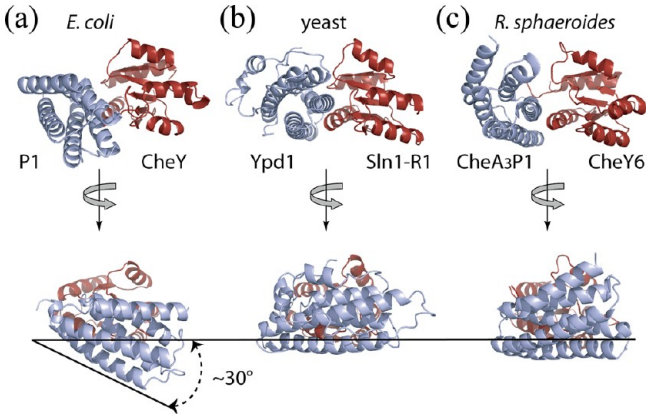

Figure 9. Comparison of the *E. coli* P1−CheY complex (a) with the yeast Ypd1−Sln1(R1) complex (b) and the *R. sphaeroides* $CheA_3P1$−$CheY_6$ complex (c). The HPt domains are colored light blue, and the RR domains, colored red, are held constant to show the difference in the relative orientation of the two domains among these structures. *E. coli* P1 appears to be rotated downward (∼30°) compared to yeast Ypd1 and *R. sphaeroides* $CheA_3P1$, so that the top of the active site surface of CheY is more exposed in the *E. coli* model (bottom row). The extent of rotation was estimated by comparing the orientation of $\alpha 1$ of *E. coli* P1 to those of its equivalent helices in the other two structures.

interacting proteins can exhibit different assembly orientations when they have sequences that are <30−40% identical.[51] For instance, there are two distinct families, one designated as the *E. coli* family and the other the *B. subtilis* family among the known structures of the CheY−P2 complexes. Both families share similar binding regions of P2 and CheY, but the P2 domain in one family is rotated by almost 90° with respect to that of the other family when the CheY parts of the complex structures are aligned.[51] There is little sequence identity between *E. coli* P1 and Ypd1 (28%) or $CheA_3P1$ (25%) or between *E. coli* CheY and SLN1(R1) (14%) or $CheY_6$ (26%). Given the low levels of sequence identity (even within their binding surfaces) the *E. coli* P1−CheY complex shares with the yeast Ypd1−SLN1 complex or the *R. sphaeroides* $CheA_3P1$−$CheY_6$ complex, it is not inconceivable that these complexes should exhibit different interaction orientations.

Moreover, careful examination of our NOE results suggests that the *E. coli* complex should show a different relative orientation of the HPt domain with respect to the RR domain. While the positions of the HPt residues responsible for interaction are equivalent in all three cases, the positions of their interaction partners on the RR side appear to be different in the *E. coli* complex. In our *E. coli* model, P1 residues F8, T11, and E15 (Figure 10a, residues colored dark red) align with the face of $\alpha 1$ of CheY that consists of residues L24, I20, and T16 (Figure 10a, residues colored blue). In the crystal structures of the yeast complex and the *R. sphaeroides* complex, the HPt residues at the same positions (although not conserved) appear to interact mostly with the RR residues equivalent to positions 16, 19, and 23 in *E. coli* CheY (Figure 10, residues colored orange), which comprise the face of the RR $\alpha 1$ adjacent to that which interacts with *E. coli* P1. This mode of interaction also allows the interactions between P1 residues M3 and I5 and the CheY loop between $\beta 5$ and $\alpha 5$ (Figure 10a, residues colored magenta) evidenced by multiple NOEs. This requires that the C-terminal end of *E. coli* P1 $\alpha 1$ be rotated downward with respect to CheY compared to the *R. sphaeroides* $CheA_3P1$ or

dx.doi.org/10.1021/bi300147m | *Biochemistry* 2012, 51, 3786−3798

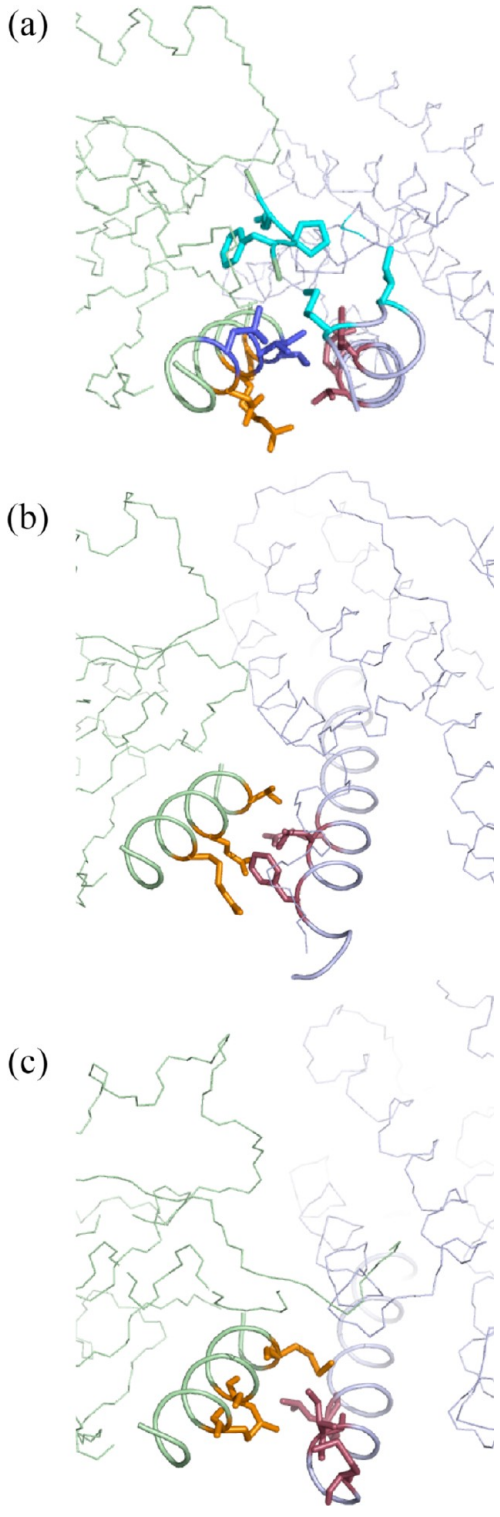

Figure 10. Comparison of HPt−RR interaction surface in the *E. coli* P1−CheY complex (a), the yeast Ypd1−Sln1(R1) complex (b), and the *R. sphaeroides* $CheA_3P1$−$CheY_6$ complex (c). HPt domains are shown on the right (grey), and RRs are shown on the left (light green). The residues responsible for the HPt interaction in yeast Sln1(R1) and *R. sphaeroides* CheY are colored orange. The interacting residues in yeast Ypd1 and *R. sphaeroides* $CheA_3P1$ are colored dark red. The equivalent positions in the *E. coli* proteins are shown in the same colors. *E. coli* CheY residues observed to be interacting with P1 are colored blue. An additional interaction between the CheY loop (residues 109−111) and M3 and I5 of P1 is colored cyan.

yeast Ypd1, which accounts for the differences in the orientation shown in Figure 9. This argument hinges on the notion that the arrangement of RR α1 with respect to the rest of the domain in these complexes is similar, which appears to be the case.

If the complex reported in this study indeed is a complex that forms during the phosphate relay from CheA to CheY, what might be its meaning? One obvious hypothesis would be that this is the complex that forms as the reaction happens. As discussed above, the distance between the active site residues clearly makes the transfer possible. Another possibility would be that the phosphotransfer reaction is actually conducted by a complex much closer to the yeast or *R. sphaeroides* complex (or other unknown complex) and that our structure represents a kind of a stand-by complex leading to such a complex. If that is the case, the fact that it eluded our detection suggests that the lifetime of such a hypothetical complex is shorter still than that of the observed complex, whose affinity is already very weak. One reason for our inability to observe such a complex would be that the HPt domain used in the NMR experiments was not activated because of the long-term instability of phosphorylated *E. coli* P1. In other HPt−RR systems where this is less of an issue, it has been reported that the complex structure of the activated proteins resembles the "inactive" complex except for the rigid-body shift of 2−3 Å that brings the domains closer to each other.[9,12,22,49,50]

The interaction surface between P1 and CheY as seen in our model (~700 Å^2, calculated by the PISA Webserver) is smaller than the equivalent surface seen in the structure of the yeast Ypd1−Sln1(R1) complex (970 Å^2), but larger than that in the structure of the *R. sphaeroides* $CheA_3P1$−$CheY_6$ complex (530 Å^2) (Figure 10). However, the P1−CheY interaction is much weaker than the interactions of these complexes. This may be a reflection of the difference in the mechanisms by which phosphotransfer is accomplished. In cases where phosphate is transferred between the HPt domain and the RR domain without the P2-like domains, it would take either a high intrinsic affinity between the participants or high concentrations of them to conduct such a bimolecular reaction in a timely manner. The binding between P1 and CheY is weak, with the K_d in the range of 5 mM, but the overall signaling response in *E. coli* chemotaxis may not suffer from it because of the presence of a covalently linked CheY-binding domain (P2). P1 is connected to P2 by a 23-residue linker and five flexible terminal residues. The length of a linker of this size (given by $r^2 = Cnl^2$, where n is the number of residues, C, the characteristic ratio, is close to 7 for n = 28, and l is 3.8 Å for the average C_α−C_α bond length) is expected to be ~53 Å, which agrees with our result of ~45 Å.[30] CheY and the P2 domain form a stable complex (K_d = 2 μM), and the linker should constrain CheY to a space surrounding P1, with the estimated effective concentration of each component being ~4 mM.[30] This means ~20% of the P1 population interacts with CheY at any time, despite the low intrinsic affinity. The interaction between P1 and CheY, as we detected, aligns the side chains of the two active site residues, P1 H48 and CheY D57, in the proximity of each other. This should enhance the rate of phosphotransfer greatly compared to that with the small-molecule phosphate donors with no specific affinity for CheY.

It should also be noted that, before interacting with CheY, P1 binds to the catalytic domain of CheA (the P4 domain) to receive the phosphoryl group at the same active site histidine, and it is almost certain that the relative affinity of P1 for P4 and

dx.doi.org/10.1021/bi300147m | *Biochemistry* 2012, 51, 3786−3798

CheY has been fine-tuned to meet the biological demand of chemotaxis signaling. The nature and affinity of the interaction among P1, CheY, and P2 reported here show how and how likely this interaction is designed to happen. Understanding how they fit with the previous round of phosphotransfer, however, would require a study conducted with a CheA construct including the kinase domain and is out of the scope of this report.

AUTHOR INFORMATION

Corresponding Author

*E-mail: dahlquist@chem.ucsb.edu. Phone: (805) 893-5468. Fax: (805) 893-4120.

Funding

This work was supported by National Institutes of Health Grant 9 R01 GM59544.

Notes

The authors declare no competing financial interest.

REFERENCES

(1) Stock, A. M., Robinson, V. L., and Goudreau, P. N. (2000) Two-component signal transduction. *Annu. Rev. Biochem. 69*, 183−215.

(2) Hamel, D. J., Zhou, H., Starich, M. R., Byrd, A., and Dahlquist, F. W. (2006) Chemical-shift-perturbation mapping of the phosphotransfer and catalytic domain interaction in the histidine autokinase CheA from *Thermotoga maritima*. *Biochemistry 45* (31), 9509−9517.

(3) Baker, M. D., Wolanin, P. M., and Stock, J. B. (2006) Systems biology of bacterial chemotaxis. *Curr. Opin. Microbiol. 9*, 187−192.

(4) Baker, M. D., Wolanin, P. M., and Stock, J. B. (2006) Signal transduction in bacterial chemotaxis. *BioEssays 28*, 9−22.

(5) Schuster, M., Silversmith, R. E., and Bourret, R. B. (2001) Conformational coupling in the chemotaxis response regulator CheY. *Proc. Natl. Acad. Sci. U.S.A. 98* (11), 6003−6008.

(6) Shukla, D., and Matsumura, P. (1995) Mutation leading to altered CheA binding cluster on a Face of CheY. *J. Biol. Chem. 270* (41), 24414−24419.

(7) Mayover, T. L., Halkides, C. J., and Stewart, R. C. (1999) Kinetic characterization of CheY phosphorylation reactions: Comparison of P-CheA and small-molecule phosphodonors. *Biochemistry 38* (8), 2259−2271.

(8) Zhou, H. Z., McEvoy, M. M., Lowry, D. F., Swanson, R. V., Simon, M. I., and Dahlquist, F. W. (1996) Phosphotransfer and CheY-binding domains of the histidine autokinase CheA are joined by a flexible linker. *Biochemistry 35* (2), 433−443.

(9) Zapf, J., Sen, U., Madhusuda, Hoch, J. A., and Varughese, K. I. (2000) A transient interaction between two phosphorelay proteins trapped in a crystal lattice reveals the mechanism of molecular recognition and phosphotransfer in signal transduction. *Structure 8* (8), 851−862.

(10) Casino, P., Rubio, V., and Marina, A. (2009) Structural insight into partner specificity and phosphoryl transfer in two-component signal transduction. *Cell 139*, 325−336.

(11) Xu, Q., Porter, S. W., and West, A. H. (2003) The yeast YPD1/SLN1 complex: iInsights into molecular recognition in two-component signaling systems. *Structure 11*, 1569−1581.

(12) Bell, C. H., Porter, S. L., Strawson, A., Stuart, D. I., and Armitage, J. P. (2010) Using structural information to change the phosphotransfer specificity of a two-component chemotaxis signaling complex. *PLoS Biol. 8* (2), e1000306.

(13) Battiste, J. L., and Wagner, G. (2000) Utilization of site-directed spin labeling and high-resolution heteronuclear nuclear magnetic resonance for global fold determination of large proteins with limited nuclear Overhauser effect data. *Biochemistry 39*, 5355−5365.

(14) Peterson, D. W., Zhou, H., Dahlquist, F. W., and Lew, J. (2008) A soluble oligomer of Tau associated with fiber formation analyzed by NMR. *Biochemistry 47* (28), 7393−7404.

(15) Lowry, D. F., Roth, A. F., Rupert, P. B., and Dahlquist, F. W. (1994) Signal transduction in chemotaxis. *J. Biol. Chem. 269* (42), 26358−26362.

(16) Swanson, R. W., Schuster, S. C., and Simon, M. I. (1993) Expression of CheA fragments which define domain encoding kinase, phosphotransfer, and cheY binding activities. *Biochemistry 32* (30), 7623−7629.

(17) McEvoy, M. M., Hausrath, A. C., Randolph, G. B., Remington, S. J., and Dahlquist, F. W. (1998) Two binding modes reveal flexibility in kinase/response regulator interactions in the bacterial chemotaxis pathway. *Proc. Natl. Acad. Sci. U.S.A. 95*, 7333−7338.

(18) Grassetti, D. R., and Murray, J. F. (1967) The use of 2,2-dithiodipyridine in the determination of glutathione and of triphosphopyridine nucleotide by enzymatic cycling. *Anal. Biochem. 12*, 427−434.

(19) Kay, L. E., Keifer, P., and Saarinen, T. (1992) Pure absorption gradient enhanced heteronuclear single quantum correlation spectroscopy with improved sensitivity. *J. Am. Chem. Soc. 114* (26), 10663−10665.

(20) Delaglio, F., Grzesiek, S., Vuister, G. W., Zhu, G., Pfeifer, J., and Bax, A. (1995) NMR Pipe: A multidimensional spectra; processing system based on UNIX pipes. *J. Biomol. NMR 6*, 277−293.

(21) Kraulis, P. J. (1989) ANSIG: A program for the assignment of protein ^{1}H 2D NMR spectra by interactive graphics. *J. Magn. Reson. 24*, 627−633.

(22) Vuister, G. W., and Bax, A. (1992) Resolution enhancement and spectral editing of uniformly ^{13}C-enriched protein by homonuclear broadband ^{13}C decoupling. *J. Magn. Reson. 98*, 428−435.

(23) Muhandiram, D. R., and Kay, L. E. (1994) Gradient-enhanced triple-resonance three-dimensional NMR experiments with improved sensitivity. *J. Magn. Reson., Ser. B 103*, 203−216.

(24) Montelione, G. T., Lyons, B. A., Emerson, S. D., and Tashiro, M. (1992) An efficient triple experiment using carbon-13 isotropic mixing for determining sequence-specific resonance assignments of isotropically-enriched proteins. *J. Am. Chem. Soc. 114*, 10974−10975.

(25) Grzesiek, S., Anglister, J., and Bax, A. (1993) Correlation of backbone amide and aliphatic side-chain resonance in ^{13}C/^{15}N-enriched proteins by isotropic mixing of ^{13}C magnetization. *J. Magn. Reson., Ser. B 101*, 114−119.

(26) Logan, T. M., Olejniczak, E. T., Xu, R. X., and Fesik, S. W. (1993) A general method for assigning NMR spectra of denatured proteins using 3D HC(CO)NH-TOCSY triple resonance experiments. *J. Biomol. NMR 3*, 225−231.

(27) Clore, G. M., and Gronenborn, A. M. (1998) Determining the structures of large proteins and protein complexes by NMR. *Trends Biotechnol. 16*, 22−34.

(28) Cai, M., Huang, Y., Zheng, R., Wei, S., Ghirlando, R., Lee, M. S., Craigie, R., Gronenborn, A. M., and Clore, G. M. (1998) Solution structure of the cellular factor BAF responsible for protecting retroviral DNA from autointegration. *Nat. Struct. Biol. 5* (10), 903−909.

(29) Kawamura, T., Le, L. U. K., Zhou, H., and Dahlquist, F. W. (2007) Solution structure of *Escherichia coli* PapI, a key regulator of the Pap Pili phase variation. *J. Mol. Biol. 365*, 1130−1142.

(30) Suh, J., Cai, M., Williams, D. C., Jr., and Clore, G. M. (2006) Solution structure of a post-transition state analog of the phosphotransfer reaction between the A and B cytoplasmic domains of the mannitol transporter II^{Mannitol} of the *Escherichia coli* phosphotransferase system. *J. Biol. Chem. 281* (13), 8939−8949.

(31) Garrett, D. S., Seok, Y., Peterkofsky, A., Gronenborn, A. M., and Clore, G. M. (1999) Solution structure of the 40,000 M_r phosphoryl transfer complex between the N-terminal domain of enzyme I and HPr. *Nat. Struct. Biol. 6* (2), 166−173.

(32) Suh, J., Iwahara, J., and Clore, G. M. (2007) Intramolecular domain- domain association/dissociation and phopsphoryl transfer in the mannitol transporter of *Escherichia coli* are not coupled. *Proc. Natl. Acad. Sci. U.S.A. 104* (9), 3153−3158.

(33) Hu, J., Hu, K., Williams, D. C., Jr., Komlosh, M. E., Cai, M., and Clore, G. M. (2008) Solution NMR structure of productive and non-productive complexes between the A and B domains of the

cytoplasmic subunit of the mannose transporter of the *Eschericia coli* phosphotransferase system. *J. Biol. Chem. 283* (16), 11024−11037.
(34) Jung, Y., Cai, M., and Clore, G. M. (2010) Solution structure of the $IIA^{Chitobiose}$-$IIB^{Chitobiose}$ complex of the *N,N′*-diacetylchitobiose branch of the *Escherichia coli* phosphertransferase system. *J. Biol. Chem. 285* (6), 4173−4184.
(35) Wang, G., Louis, J. M., Sondej, M., Seok, Y., Peterkofsky, A., and Clore, G. M. (2000) Solution structure of the phosphoryl transfer complex between the signal transducing proteins HPr and $IIA^{Glucose}$ of the *Escherichia coli* phosphoenolpyruvate:sugar phosphotransferase system. *EMBO J. 19* (21), 5635−5649.
(36) Cornilescu, G., Lee, B. R., Cornilescu, C. C., Wang, G., Peterkofsky, A., and Clore, G. M. (2002) Solution structure of the phosphoryl transfer complex between the cytoplasmic A domain of the mannnitol transporter $II^{Mannitol}$ and HPr of the *Escherichia coli* phosphotransferase system. *J. Biol. Chem. 277* (44), 42289−42298.
(37) Cai, M., Williams, D. C., Jr., Wang, G., Lee, B. R., Peterkofsky, A., and Clore, G. M. (2003) Solution structure of the phosphoryl transfer complex between the signal-transducing protein $IIA^{Glucose}$ and the cytoplasmic domain of the glucose transporter $IICB^{Glucose}$ of the *Escherichia coli* glucose phosphotransferase system. *J. Biol. Chem. 278* (27), 25191−25206.
(38) Williams, D. C., Jr., Cai, M., Suh, J., Peterkofsky, A., and Clore, G. M. (2005) Solution NMR structure of the 48-kDa $IIA^{Mannose}$-HPr complex of the *Escherichia coli* mannose phosphotransferase system. *J. Biol. Chem. 280* (21), 20775−20784.
(39) Mourey, L., Re, S. D., Pedelacq, J., Tolstykh, T., Faurie, C., Guillet, V., Stock, J. B., and Samama, J. (2001) Crystal structure of the CheA histidine phosphotransfer domain that mediates response regulator phosphorylation in bacterial chemotaxis. *J. Biol. Chem. 276* (33), 31074−31082.
(40) Brunger, A. T. (1992) *A System for X-ray Crystallography and NMR. X-PLOR*, version 3.1, Yale University Press, New Haven, CT.
(41) Zhou, H., and Dahlquist, F. W. (1997) Phosphotransfer site of the chemotaxis-specific protein kinase CheA as revealed by NMR. *Biochemistry 36* (4), 699−710.
(42) Stewart, R. C., Jahreis, K., and Parkinson, J. S. (2000) Rapid phosphotransfer to CheY from a CheA protein lacking the CheY-binding domain. *Biochemistry 39* (43), 13157−13165.
(43) Frost, A. A., and Pearson, R. G. (1965) *Kinetics and Mechanism*, 2nd ed., pp 166, John Wiley & Sons, Inc., New York.
(44) Welch, M., Chinardet, N., Mourey, L., Birck, C., and Samama, J. (1998) Structure of the CheY-binding domain of histidine kinase CheA in complex with CheY. *Nat. Struct. Biol. 5* (1), 25−29.
(45) Gouet, P., Chinardet, N., Welch, M., Guillet, V., Cabantous, S., Birck, C., Mourey, L., and Samama, J. (2001) Further insights into the mechanism of function of the response regulator CheY from cystallorgraphic studies of the CheY-CheA124−257 complex. *Acta Crystallogr. D57*, 44−51.
(46) Li, J., Swanson, R. V., Simon, M. I., and Weis, R. M. (1995) The response regulators CheB and CheY exhibit competitive binding to the kinase CheA. *Biochemistry 34* (45), 14626−14636.
(47) McEvoy, M. M., Muhandiran, D. R., Kay, L. E., and Dahlquist, F. W. (1996) Structure and dynamics of a CheY- binding domain of the chemotaxis kinase CheA determined by nuclear magnetic resonance spectroscopy. *Biochemistry 35* (18), 5633−5640.
(48) Volz, K., and Matsumura, P. (1991) Crystal structure of *Escherichia coli* CheY refined at 1.7-Å resolution. *J. Biol. Chem. 266* (23), 15511−15519.
(49) Varughese, K. I., Tsigelny, I., and Zhao, H. (2006) The crystal structure of beryllofluoride Spo0F in complex with the phosphotransferase Spo0B represents a phosphotransfer pretransition state. *J. Bacteriol. 188* (13), 4970−4977.
(50) Zhao, X., Copeland, D. M., Soares, A. S., and West, A. H. (2008) Crystal structure of a complex between the phosphorelay protein YPD1 and the response regulator domain of SLN1 bound to a phosphoryl analog. *J. Mol. Biol. 375* (4), 1141−1151.
(51) Park, S., Beel, B. D., Simon, M. I., Bilwes, A. M., and Crane, B. R. (2004) In different organisms, the mode of interaction between two signaling proteins is not necessarily conserved. *Proc. Natl. Acad. Sci. U.S.A. 101* (32), 11646−11651.

NOTE ADDED AFTER ASAP PUBLICATION

This paper was published on the Web on April 26, 2012. The second paragraph was revised with additional clarifying content and the corrected version was reposted on May 8, 2012.